A Shock-Tube Laser-Schlieren Study of the Decomposition of Diacetyl

Robert S. Tranter*, Xueliang Yang
Chemical Sciences and Engineering Division
Argonne National Laboaratory
Argonne, IL-60439

John H. Kiefer
Department of Chemical Engineering
University of Illinois at Chicago
Chicago, IL-60607

Ahren W. Jasper
Combustion Research Facility
Sandia National Laboratory
Livermore, CA-94551

Abstract

The dissociation of diacetyl dilute in krypton has been studied in a shock tube using laser schlieren densitometry, LS, at 1200-1800 K and at two reaction pressures, 55±2 Torr and 120±3 Torr. The experimentally determined rate coefficients show falloff. An *ab-initio*/Master Equation/VRC-TST analysis was used to determine pressure dependent rate coefficient expressions that are in good agreement with the experimental data. $k(T)_{120\mathrm{Torr}} = 1.32 \times 10^{34}\ (T/300\ \mathrm{K})^{-20.3} \exp(-50482/T)\ \mathrm{s}^{-1}$ and $k(T)_{55\mathrm{Torr}} = 1.59 \times 10^{33}\ (T/300\ \mathrm{K})^{-19.9} \exp(-48972/T)\ \mathrm{s}^{-1}$. The LS profiles were simulated using a model for methyl recombination with appropriate additions for diacetyl. Excellent agreement is found between the simulations and experimental profiles.

Introduction

The dissociation of diacetyl, 2,3-butadione, is initiated by C-C fission, R1, to form two acetyl radicals.

$$CH_3COCOCH_3 \rightarrow CH_3CO + CH_3CO \qquad (1)$$

The earliest reports on the thermal decomposition of diacetyl are by Rice and Walters [1] (420-470 K, 38-458 Torr) and Walters [2] (383-436 K, 147-287 Torr) who studied the reaction in bulb experiments. Product analyses were performed and a reaction mechanism proposed along with rate coefficients for (1). Subsequent thermal experiments were carried out in a stirred flow reactor (677-776 K, 0.6-45 Torr) by Hole and Mulcahy [3] and in a flow tube by Scherzer and Plarre [4] (822-905 K, 0.6-430 Torr). Knoll et al [5] investigated R1 in static cells (648-690 K, 43-183 Torr). The rate coefficients for reaction (1) obtained by Knoll et al., Hole and Mulcahy and, Scherzer and Plarre are in good agreement.

Based on product analyses from the above investigations and experimental studies by Guenther et al. [6], Blacet [7] and Bell and Blacet [8] a reaction mechanism for the low temperature pyrolysis of diacetyl has been elucidated that satisfactorily explains the main products ketene, methane, acetone, ethane and CO. The previous studies indicate that (1) is the sole dissociation path for diacetyl but that the rapid decomposition of the acetyl radical via (2) promotes a chain reaction mechanism propagated by methyl radicals.

$$CH_3CO \rightarrow CH_3 + CO \qquad (2)$$
$$CH_3 + CH_3COCOCH_3 \rightarrow CH_4 + CH_2COCOCH_3 \qquad (3)$$
$$CH_3 + CH_3COCOCH_3 \rightarrow CH_3COCH_3 + CH_3CO \qquad (4)$$
$$CH_3 + CH_3 \rightarrow C_2H_6 \qquad (5)$$

Methyl radicals attack the parent molecule via (3) and (4) and the $CH_2COCOCH_3$ radical formed in (3) readily dissociates to ketene and CH_3CO. At the low temperatures of these studies methyl recombination (5) is the main termination step.

There are no high temperature studies of diacetyl pyrolysis in the literature and at elevated temperatures the mechanism may be complicated by reactions of H atoms generated from secondary reactions of CH_3 and dissociation of ketene, Although, from Frank et al. [9]

* Corresponding author: tranter@anl.gov

ketene may be relatively stable in the temperature range of the current work .

The dissociation of acetyl radicals, (2), is the primary source of CH_3 radicals in diacetyl pyolysis. At shock tube temperatures the only experimental value for dissociation of the acetyl radical is a recent estimate by Yasunaga et al. [10] which was derived from a shock tube study of acetaldehyde pyrolysis. Recommended rate coefficients for (2) also appear in compilations of kinetic data such as those of Baulch et al. [11]. Reaction (2) has also been the subject of three recent theoretical investigations by Huynh et al. [12], Senosiain et al. [13] and Lee and Bozzelli [14], with calculated rate coefficients covering the range 200-2500 K. Senosiain et al. estimated pressure dependent rate coefficients that are in good agreement with the low temperature experimental results and demonstrate that dissociation of acetyl via (2) is the only viable route at high temperatures with all other pathways having significantly higher barriers.

Given the above considerations dicetyl pyrolyis appears to be an attractive, clean pyrolytic source of methyl radicals at shock tube temperatures and it may be superior to some other sources we have used: ethane, acetaldehyde and acetone. The easiest of these other precursors to dissociate, acetone, has about a 10 kcal/mol higher bond strength, so diacetyl should be usable for methyl formation at somewhat lower temperatures. Also, with the diacetyl, its shorter lifetime should reduce the effect of interfering abstraction reactions.

Specific Objectives

The study of the diacetyl dissociation and the subsequent recombination of the resulting methyl radicals are well suited to investigation by the laser-schlieren shock tube technique. The measured beam deflections are proportional to the net endothermic rate and will generate large initial positive gradients from (1) followed by strong negative gradients arising mainly from methyl recombination, (5). The two processes are well-separated in time as well as sign and can be clearly seen and differentiated. Both initial diacetyl decomposition rates and an expanded and verified mechanism for the methyl recombination and its associated chain mechanism are presented here. Some theory of the decomposition and RRKM modeling are also presented

Experimental

The LS experiments were performed in a diaphragmless shock tube, DFST, which has been fully described elsewhere [15]. The driver section of the DFST contains a fast acting valve which replaces the more traditional diaphragm, Fig. 1. When the valve is closed by pressurizing the inside of the bellows, the driver and driven sections are separated and can be filled to the desired loading pressures and the DFST is fired by rapidly opening the valve. By varying both the driver section pressure, P_4, and the driven section pressure, P_1, the pressure behind the incident shock wave, P_2, can be constrained to very narrow ranges, typically < ±3%, over a wide range of temperatures [15].

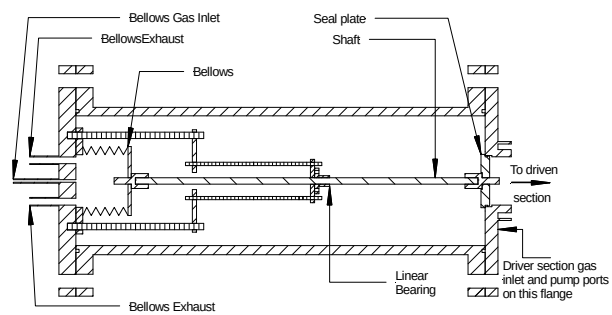

Figure 1: Schematic of the diaphragmless shock tube driven section.

The driven section of the shock tube has an internal diameter 7.01 cm and the quartz windows, through which the beam from a helium-neon laser passes for LS measurements, are located sufficiently far downstream to allow the shock wave to be fully developed after firing the DFST. A set of six pressure transducers evenly spaced along the side of the driven section are centered around the LS windows, and incident shock wave velocities were obtained by interpolation of five intervals calculated from measured times centered about the LS beam. From these velocities and the loading conditions the temperature and pressure behind the incident shock wave are calculated assuming frozen conditions. The uncertainty in velocity is estimated as 0.2%, corresponding to a temperature error of less than 0.5%, here amounting to the order of 10-15K.

The LS diagnostics and technique have also been thoroughly described previously [16,17]. The molar refractivity of Kr = 6.367 [18], while that of diacetyl=20.99 was calculated from its refractive index and molar density. The usual assumption is made that the mixture molar refractivity does not vary significantly with extent of reaction.

Mixtures containing 1% and 2% dicetyl dilute in krypton were prepared manometrically in a 50 L glass vessel that had been evacuated to $<10^{-3}$ Torr. Krypton (AGA 99.999%), was used as supplied. Diacetyl (Aldrich Chemical Co., 99%) was degassed by repeated freeze–pump–thaw cycles with liquid nitrogen. Reagent mixtures were allowed to homogenize for several hours before use.

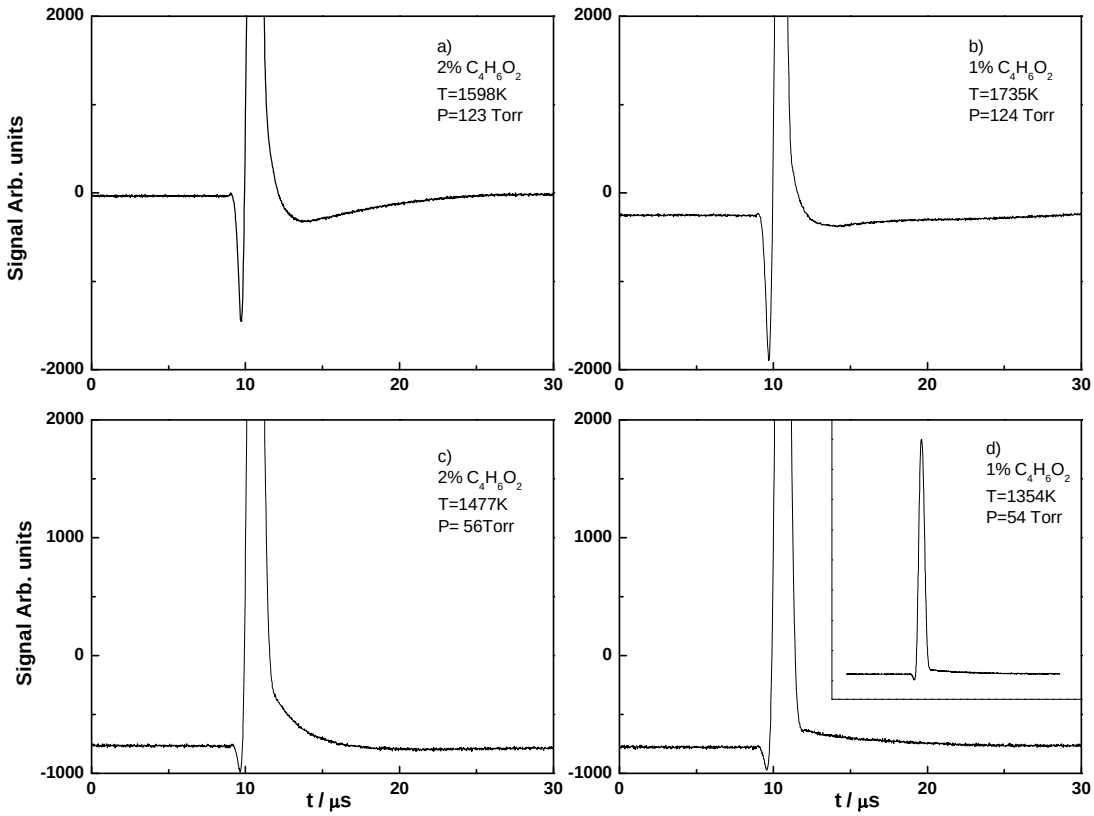

Figure 2: Example raw signals from LS experiments with 1 and 2% diacetyl dilute in krypton. The figures have been expanded vertically to show the curvature due to reaction more clearly. The inset figure in (d) shows the complete signal.

Theory

The capture (high pressure limit) kinetics for the self-recombination of CH_3CO were computed using direct variable reaction coordinate transition state theory [19-21] (VRC-TST), as implemented in the computer code VaReCoF [22] The interaction potential energy surface was evaluated on-the-fly using the CASPT2 method, the cc-pVDZ basis set corrected using the one-dimensional correction for C–C bond-forming reactions developed elsewhere [23], and a two-electron, two-orbital active space. Dividing surfaces were constructed by placing pivot points at the center of mass of the fragments, at the reactive C atom, or displaced from the reactive C atom in the direction of the radical orbital by 0.3 or 0.5 Å. For each pivot point type, pivot point separations from ~3–10 Å were included in the microcanonical variational optimizations.

Master equation (ME) calculations [24] for diacetyl decomposition were carried out using the VRC-TST kinetics and B3LYP/6-311++G(d,p) frequencies and geometries for diacetyl. The resulting rate coefficients were found to be in the falloff region at the pressures of interest (55–120 Torr), and the results are therefore sensitive to the bond energy (E_0) and to the energy transfer parameters used in the ME calculations. Consequently, these parameters were optimized to reproduce the experimental data.

Results and Discussion

A total of 80 ST/LS experiments have been performed over the temperature range $1200 < T_2 < 1800$ K and $P_2 = 55 \pm 2$ Torr and $P_2 = 120 \pm 3$ Torr using both 1% and 2% mixtures of diacetyl dilute in krypton at both reaction pressures. Examples of the raw laser schlieren profiles covering the complete experimental range are shown in Fig. 2. All of the profiles have several common features. The large, positive spike and the preceding negative spike are due to diffraction and refraction of the laser beam as the shock front passes

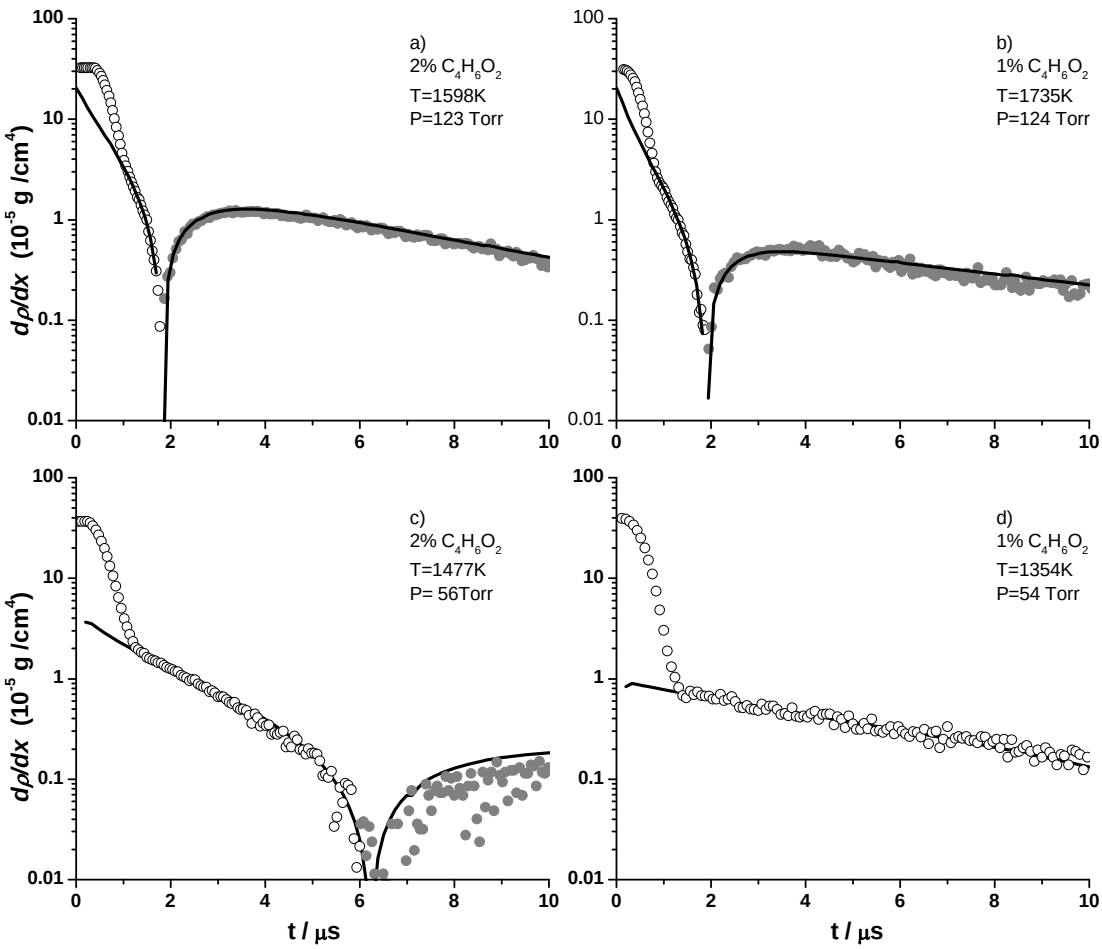

Figure 3: Semi-log density gradient plots derived from the raw LS signals shown in Fig.2. Absolute values are plotted and open symbols represent positive values and closed symbols represent negative values. The symbols represent experimental data and the lines are results of simulations using the model in Table 1with optimum value for R1, R2 and R31.

through it [25]. The remaining signal to the right of the large spike is due to chemical reaction. In the lower pressure and lower temperature experiments, e.g. Figs. 2c and d, there is a sharp excursion in the signal whereas in the experiments where the initial dissociation is more rapid this break in the signal can be harder to identify, see for example Fig. 2a. However the break is usually easy to identify on semi-log plot like those of Figs. 3 a and b. The top two plots in Fig. 2 also show minima that dip below the signal which precedes arrival of the shock wave, used to define the baseline in each experiment. Minima like these in LS signals are characteristic of net exothermic processes.

The raw signals are converted into density gradients and examples of the density gradient / time plots, corresponding to the experiments show in Fig. 2, are presented in semi-log form in Fig. 3. The first few points in each figure are due to the end portion of the shock front / laser beam interaction described above. Unfortunately, this masks the location of t_0, the time origin at the onset of reaction. Consequently, t_0 is located by a well established method [25]. Typically, the time origin is located to an accuracy of 0.1 – 0.2 µs and the corrections are largest for the lowest pressure experiments where there is greater curvature in the shock front.

Most of the density gradient profiles obtained in the diacetyl experiments show a rapid change from positive to negative density gradients before recovering to the baseline at long reaction times, a few microseconds. At the time origin the only reaction contributing to the density gradient is the initial

dissociation of diacetyl and by extrapolating the density gradient profiles back to t_0 accurate estimates for the rate coefficient, k_1, are obtained. For experiments where the initial rates of reaction are fairly small, e.g. Figs. 3c and d, this extrapolation is quite accurate. However, as the rate increases the extrapolation becomes somewhat less precise. Consequently, the initial estimates are refined by a well established iterative procedure involving simulation of the whole of the density gradient profile that accounts for changes in reaction temperature and the contribution of secondary reactions. The mechanism used to simulate the LS profiles is presented in Table I and hereon reaction numbers prefixed by R correspond to those given in Table I. Normally, the initial estimates for R1 do not change by more than 10-20%.

In a number of the 55 Torr experiments the optimized simulation results run close to the experimental data but parallel it on the underside. Experience has shown that this is not due to deficiencies in the mechanism but due to either error in the location of t_0, most significant at low pressure, or due to incubation. In diacetyl/Kr mixtures relaxation is very fast and indeed we have been unable to resolve it even at very low temperatures and pressures. Our best estimates of incubation times at 55 Torr are 0.1-0.2 µs similar to the error in t_0. Consequently, for experiments such as those shown in Fig. 3c and d the start of simulation has been delayed accordingly.

The first order rate coefficients determined from the 55 Torr and 120 Torr LS experiments are presented in Fig. 4 where they are also compared to the theoretical values determined from the ME/VRC-TST work. Clearly, the rate coefficients show a strong fall off from the theoretical high pressure limiting rate coefficient and the small pressure dependency between the two sets of experimental results is well resolved. This resolution is due, at least in part, to the control over reaction conditions obtainable with the DFST.

It was noted above that the results of the ME analysis would be sensitive to both E_0 and the energy transfer parameter. The experimental data were fitted very well using E_0 = 70.0 kcal/mol and a temperature dependent energy transfer parameter $a(T) = 300\ (T/300\ \mathrm{K})^{0.7}\ \mathrm{cm}^{-1}$, Fig. 4. The fitted bond energy is in good agreement with a value calculated from literature values of $\Delta H_{f,0}$ for diacetyl and acetyl radicals [26] (72.0 ± 2.8 kcal/mol) and the present calculated QCISD(T)/CBS//B3LYP/6-311++G(d,p) values (72.6 kcal/mol). The fitted energy transfer parameters are somewhat larger than those derived in a recent study of methanol decomposition [27], which is reasonable as the efficiency of energy transfer is likely to increase with the size of the system. The calculated rate coefficients for 55 Torr and 120 Torr were fit to modified Arrhenius forms for 1200–1800 K and a

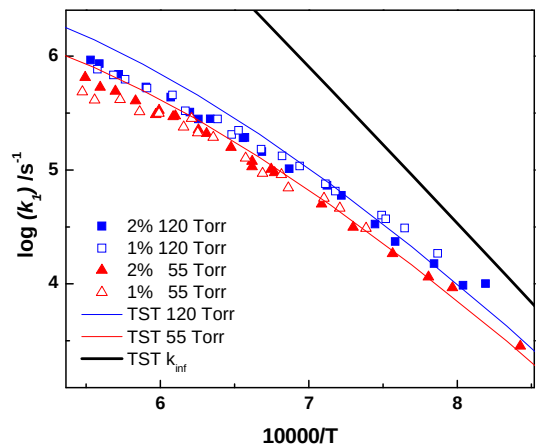

Figure 4*:* Comparison of experimental rate coefficients for reaction (1) and the results of ME calculations with E_0=70 kcal/mol and α(T) as given in the text. Symbols are experimental points and lines represent calculations.

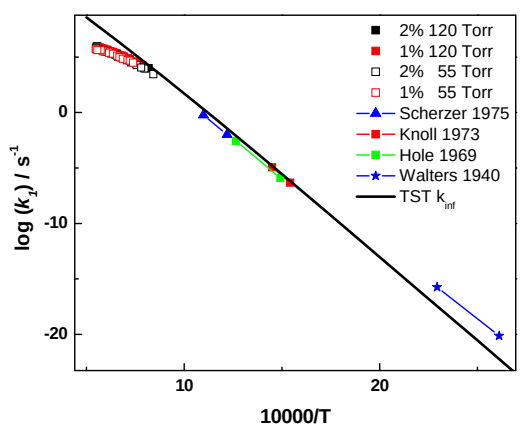

Figure 5: Comparison of the k_∞ from ME calculations with literature data for reaction (1). The points are the experimental values from the current work at 55 and 120 Torr.

comparison with the current experimental work is given in Fig.4.

$k_{55Torr}(T) = 1.59\mathrm{x}10^{33}\ (T/300\ \mathrm{K})^{-19.9}\ \exp(-48972/T)\ \mathrm{s}^{-1}$

$k_{120Torr}(T) = 1.32\mathrm{x}10^{34}\ (T/300\ \mathrm{K})^{-20.3}\ \exp(-50482/T)\ \mathrm{s}^{-1}$

$k_\infty(T) = 1.325\ \mathrm{x}10^{19}\ (T/300\ \mathrm{K})^{-3.287}\ \exp(-36150\ /T)\ \mathrm{s}^{-1}$ and is valid for 300-2000K

Table I: Reaction mechanism and Arrhenius parameters for Diacetyl pyrolysis. Units: kcal/mol, mole, cm^3, s. the values shown for R1, R2 and R31, highlighted in red, have been optimized for 120 Torr.

	Reaction	logA	n	E_a	Reference	ΔH
R1	$CH_3COCOCH_3$+M =CH_3CO+CH_3CO+M	45.300	-8.00	60.5	This work	72.9
R2	C_2H_6 + M = CH_3 + CH_3 + M	18.900	0.00	74.0	This work	90.2
R3	C_2H_6 + H = C_2H_5 + H_2	1.500	3.50	5.2	[30]	-3.5
R4	C_2H_6 + CH_3 = C_2H_5 + CH_4	-0.261	4.00	8.3	[30]	-4.3
R5	CH_3 + CH_3 = C_2H_5 + H	13.732	0.00	16.1	[11]	10.6
R6	C_2H_4 + H = C_2H_5	40.870	-8.81	11.6	[31]	-36.0
R7	C_2H_4 + H = C_2H_3 + H_2	7.703	1.93	13.0	[31]	5.4
R8	CH_4 + M = CH_3 + H + M	47.219	-8.00	121.5	[32]	105.0
R9	C_2H_4 + M = C_2H_2 + H_2 + M	17.310	0.00	78.3	[31]	42.0
R10	C_2H_4 + M = C_2H_3 + H + M	17.413	0.00	96.6	[31]	110.4
R11	C_2H_5 + H = C_2H_4 + H_2	12.300	0.00	0.0	[33]	-68.2
R12	C_2H_2 + H = C_2H_3	30.248	-5.98	6.0	[31]	-35.8
R13	C_2H_3 + H = C_2H_2 + H_2	13.600	0.00	0.0	[11]	-68.4
R14	CH_4 + H = CH_3 + H_2	5.7780	2.50	9.7	[32]	0.8
R15	CH_2(T) + CH_3 = C_2H_4 + H	15.070	-0.34	0.2	[34]	-63.9
R16	CH_4 + CH_2(T) = CH_3 + CH_3	6.390	2.00	8.3	[30]	-5.5
R17	CH_2(S) + H_2 = H + CH_3	13.800	-0.00	0.0	[11]	-15.3
R18	CH_3 + M = CH_2(T) + H + M	16.000	0.00	90.6	[11]	110.5
R19	C_3H_8 + M = CH_3 + C_2H_5 + M	18.892	0.00	64.9	[34]	88.7
R20	CH_3 + C_2H_5 = C_2H_4 + CH_4	11.950	0.00	0.0	[11]	-69.0
R21	H + H + M = H_2 + M	18.000	-1.00	0.0	[11]	-104.2
R22	C_2H_6 = H + C_2H_5	42.519	-8.07	110.4	[35]	100.8
R23	CH_2(S) + CH_4 = CH_3 + CH_3	13.204	0.00	-0.6	[33]	-44.9
R24	CH_2(S) + CH_3 = C_2H_4 + H	13.079	0.00	-0.6	[33]	-72.8
R25	CH_2(S) + M = CH_2(T) +M	12.950	0.00	0.6	[33]	-9.0
R26	CH_2(S) + C_2H_6 = CH_3 + C_2H_5	13.600	0.00	-0.6	[33]	-18.8
R27	CH_2(T) + CH_2(T) = C_2H_2 + H_2	13.500	0.00	-0.0	[33]	-132.5
R28	CH_2(T) + H_2 = H + CH_3	5.700	2.00	7.2	[33]	-6.3
R29	CH_3CO = CH_3 + CO	16.500	-2.09	15.2	[13]	11.1
R30	$CH_3COCOCH_3$+H=CH_3CO+ CH_2CO +H_2	7.962	2.00	5.0	[36]	12.2
R31	$CH_3COCOCH_3$+CH_3=CH_3CO+CH_2CO +CH_4	0.450	4.00	7.9	This work	11.4
R32	CH_2CO = CH_2(T) + CO	15.361	0.00	57.6	[9]	78.1
R33	CH_2CO + H = CH_3 + CO	8.900	1.45	2.8	[13]	-32.4
R34	CH_2CO + CH_3 = C_2H_5 + CO	12.699	0.00	0.0	[37]	-21.8
R35	CH_3COCH_3 = CH_3 + CH_3CO	16.400	0.00	81.7	[36]	83.9
R36	CH_3 + CH_3CO= C_2H_6 + CO	13.600	0.00	0.0	[38]	-56.9

The theoretical calculations predict pressure dependence from 55–120 Torr and the magnitude is in agreement with that found experimentally. The temperature dependence in the theoretical rate coefficients is predicted to be somewhat larger than what is observed experimentally, and we note that the predicted temperature dependence can be improved by using a lower value of E_0 = 68.2 kcal/mol with $a(T)$ = 215 $(T/300\ K)^{0.7}$ cm^{-1}. However, as the lower E_0 is outside the reported uncertainty based on $\Delta H_{f,0}$ from literature values and the fit with E_0=70.0 kcal/mol is satisfactory we prefer to use the higher value at this time.

The high pressure limit rate coefficient has also been compared with the low temperature experimental results of Scherzer and Plarre [4], Knoll et al. [5] and Hole et al [3] in Fig. 5. Clearly, the agreement is very good.

Modeling

In Fig.3 simulations of the experimental profiles are shown. These were performed using a computer code designed to model reactive flows behind shock waves using a methodology similar to that outlined by Gardiner [28]. The simulations account for temperature changes as the reaction progresses and reverse reactions are included for all reactions through the equilibrium constants and detailed balance. The model used is presented in Table I and essentially consists of two parts, namely a portion that describes the chemistry associated with diacetyl, R1 and

R29-R36, and a sub mechanism that describes the reactions related to methyl radicals. The later part has been taken directly from a recent study on the dissociation of methyliodide [29] using LS over a similar range of temperature. During the simulations R1, R2 and R31 were varied to optimize the fit to the experimental profiles with all other rate coefficients being fixed and where appropriate rate coefficient expressions for each reaction pressure have been used [29].

The initial part of the LS profile is sensitive only to R1 as described above. R2 represents the recombination of methyl radicals and the location and depth of the minima, Fig. 3, are very sensitive to this rate. The optimized values for R2 do not vary by more than ± 10% compared to those determined in reference [29]. R31 is a combination of (3) and (4) assuming rapid dissociation of the radical product of (3). While R31 itself does not contribute directly to the density gradient due to the small heat of reaction it does affect the profile by regenerating methyl radicals and ketene. Under the conditions of the current work, unlike the earlier low temperature studies, ketene dissociates via R32 to generate methylene and it also reacts with H and CH_3 via R33 and R34 respectively. These reactions are more significant at high temperatures and play a role in determining the shape of the later part of the density gradient profile that cannot be ignored.

Over the whole range of experiments the fit between the experimental profiles and the simulation results is excellent as shown in Fig. 3.

Conclusions

The dissociation of diacetyl has been studied at high temperatures and low pressures in a shock tube significantly extending the range of experimental conditions. The initial dissociation is in the fall off range and a theoretical model has been constructed that correctly predicts the pressure dependence and provides a good fit to the experimental results using reasonable estimates of E_0 and the downward energy transfer parameter.

A mechanism for the high temperature dissociation of diacetyl has also been developed and excellent agreement between the model and experimental LS profiles is obtained. At low temperatures the contributions from potentially interfering reactions R31 and R32 are very minor as is any contribution from R32, ketene dissociation. However, at the higher temperatures of this work these reactions while minor are not negligible. Consequently, dicetyl pyrolysis can be considered as quite a clean, efficient source of methyl radicals below around 1500 K particularly when low dilutions of reagent are employed.

Acknowledgments

This work was performed under the auspices of the Office of Basic Energy Sciences, Division of Chemical Sciences, Geosciences, and Biosciences, U.S. Department of Energy, under contract numbers DE-AC02-06CH11357, DE-AC04-94-AL85000, DE-FE-85ER13384

References

[1] F.O.Rice and W.D.Walters, J. Chem. Phys. **7** (1939) 1015-1018.

[2] W.D.Walters, J.Am.Chem.Soc. **62** (1940) 880-886.

[3] K.J.Hole and M.F.R.Mulcahy, J. Phys. Chem. **73** (1969) 177-185.

[4] K.Scherzer and D.Plarre, Zeit. Phys. Chem. **256** (1975) 660-672.

[5 K.S.Knoll, Int. J. Chem. Kinet. **5** (1973) 271-283.

[6] W.B.Guenther, C.A.Whiteman and W.D.Walters, J.Am.Chem.Soc. **77** (1955) 2191-2192.

[7] F.E.Blacet and W.E.Bell, Disc. Faraday Soc. **14** (1954) 70-76.

[8] W.E.Bell and F.E.Blacet, J.Am.Chem.Soc. **76** (1954) 5332-5337.

[9] P.Frank, K.A.Bhaskaran and T.Just, J.Phys.Chem. **90** (1986) 2226-2231.

[10] K.Yasunaga, S.Kubo, H.Hoshikawa, T.Kamesawa and Y.Hidaka, Int. J. Chem. Kinet. **40** (2008) 73-102.

[11] D.L.Baulch, C.T.Bowman, C.J.Cobos, R.A.Cox, T.Just, J.A.Kerr, M.J.Pilling, D.Stocker, J.Troe, W.Tsang, R.W.Walker and J.Warnatz, J.Phys.Chem.Ref.Data **34** (2005) 757-1397.

[12] L.K.Huynh and A.Violi, J. Org. Chem. **73** (2008) 94-101.

[13] J.P.Senosiain, S.J.Klippenstein and J.A.Miller, J.Phys.Chem.A **110** (2006) 5772-5781.

[14] J.Lee and J.W.Bozzelli, Int. J. Chem. Kinet. **35** (2003) 20-44.

[15] R.S.Tranter and B.R.Giri, Rev. Sci. Instrum. **79** (2008).

[16] J.H.Kiefer and A.C.Manson, Rev. Sci. Instrum. **52** (1981) 1392-1396.

[17] J.H.Kiefer, in: A.Lifshitz (Ed.), Shock Waves in Chemistry Marcel Dekker, New York, 1981, pp. 219-277.

[18] W.C.Gardiner, Y.Hidaka and T.Tanzawa, Combust. Flame **40** (1981) 213-219.

[19] S.J.Klippenstein, J. Chem. Phys. **96** (1992) 367-371.

[20] S.J.Klippenstein, J.Phys.Chem. **98** (1994) 11459-11464.

[21] Y.Georgievskii and S.J.Klippenstein, J. Chem. Phys. **118** (2003) 5442-5455.

[22] Y.Georgievskii and S.J.Klippenstein, in: VaReCoF, Sandia National Loboratory and Argonne National Laboratory 2008.

[23] S.J.Klippenstein, Y.Georgievskii and L.B.Harding, Phys. Chem. Chem. Phys. **8** (2006) 1133-1147.

[24] J.A.Miller and S.J.Klippenstein, J.Phys.Chem.A **110** (2006) 10528-10544.
[25] J.H.Kiefer, M.Z.Al-alami and J.C.Hajduk, Appl. Optics **20** (1981) 221-230.
[26] Burcat A. and Ruscic B., ftp://ftp.technion.ac.il/pub/supported/aetdd/thermodynamics, Ideal Gas Thermochemical Database with updates from Active Thermochemical Tables, March 2009,
[27] A.W.Jasper, S.J.Klippenstein, L.B.Harding and B.Ruscic, J.Phys.Chem.A **111** (2007) 3932-3950.
[28] W.C.Gardiner, Walker B.F. and Wakefield C.B., in: A.Lifshitz (Ed.), Shock Waves in Chemistry Marcel Dekker inc, New York, 1981, pp. 319-374.
[29] R.S.Tranter, Yang X and Goldsmith C.F., "Characterization of the Thermal Dissociation of Methyl Iodide as a Methyl Radical Source for Shock Tube Studies with Laser Schlieren and Time-of-Flight Mass Spectrometry", Proceedings of the 6th US National Meeting (The Combustion Institute, 2009).
[30] J.H.Kiefer, S.Santhanam, N.K.Srinivasan, R.S.Tranter, S.J.Klippenstein and M.A.Oehlschlaeger, Proc.Combust. Inst. **30** (2005) 1129-1135.
[31] J.A.Miller and S.J.Klippenstein, Phys. Chem. Chem. Phys. **6** (2004) 1192-1202.
[32] J.W.Sutherland, M.C.Su and J.V.Michael, Int. J. Chem. Kinet. **33** (2001) 669-684.
[33] D.F.Davidson, M.D.Dirosa, E.J.Chang, R.K.Hanson and C.T.Bowman, Int. J. Chem. Kinet. **27** (1995) 1179-1196.
[34] A.W.Jasper, S.J.Klippenstein and L.B.Harding, J.Phys.Chem.A **111** (2007) 8699-8707.
[35] P.H.Stewart, C.W.Larson and D.M.Golden, Combustion and Flame **75** (1989) 25-31.
[36] K.Sato and Y.Hidaka, Combust. Flame **122** (2000) 291-311.
[37] Woods T. and Haynes B.S., in: Proc. Combust. Inst. **25** (1994). 909-917.
[38] H.Adachi, N.Basco and D.G.L.James, Int. J. Chem. Kinet. **13** (1981) 1251-1276.